

Effect of prior laser microstructural refinement on the formation of amorphous layer in an $\text{Al}_{86}\text{Co}_{7.6}\text{Ce}_{6.4}$ alloy

C.L. Li¹, J.W. Murray², K.T. Voisey^{1,}, A.T. Clare², D.G. McCartney¹*

1: Materials, Mechanics and Structures Research Division, Faculty of Engineering, The University of Nottingham, Nottingham NG7 2RD, UK.

2: Precision Manufacturing Centre, Faculty of Engineering, The University of Nottingham, Nottingham NG7 2RD, UK.

Contact: *C.L. Li*: emxcl@nottingham.ac.uk, *J.W. Murray*: epxjm2@nottingham.ac.uk, *K.T. Voisey* (Corresponding author): katy.voisey@nottingham.ac.uk, Tel.: +44 115 951 4139; Fax: +44 115 951 3600, Postal Address: Room A30a Coates, UniversityPark, Nottingham, NG7 2RD, UK, *A.T. Clare*: adam.clare@nottingham.ac.uk, *D.G. McCartney*: graham.mccartney@nottingham.ac.uk

Abstract

Laser surface melting (LSM) pre-treatment was conducted before large area electron beam (LAEB) treatment in an attempt to eliminate the cracking of the amorphous layer. In our previous work, LAEB treatment successfully generated an amorphous layer on a cast polycrystalline Al-Co-Ce glass forming alloy. However, cracking was found and was associated with large and brittle $\text{Al}_8\text{Co}_2\text{Ce}$ phase in the bulk material. Results show that prior LSM treatment in this present work can effectively refine the microstructure of as-cast material, decreasing the particle size and particle spacing of $\text{Al}_8\text{Co}_2\text{Ce}$ phase. This decrease in the microstructural length scale greatly reduced the results of cracking of the amorphous layer. The LAEB pulse number required for the homogenisation and amorphisation of treated layer was also decreased for the laser pre-treated sample compared to as-cast material.

Keywords

electron beam, laser microstructural refinement, amorphous, glass-forming alloy, homogenisation, amorphisation, crystallisation, cracking

1 Introduction

Amorphous metallic alloys are capable of exhibiting attractive mechanical and chemical properties, especially corrosion resistance compared to the crystalline form of the same material. The Al-TM (transition metal)-RE (rare earth) family of amorphous alloys is particularly promising for corrosion resistant applications [1]. Due to their wide range of glass forming compositions and tuneable corrosion resistance, Al-Co-Ce alloys have attracted attention from corrosion protection engineers and scientists [2]. However, the high critical cooling rate required to achieve the amorphous state limits the dimensions of bulk samples. Therefore, there is interest in using surface modification techniques to generate amorphous coatings or films from these alloys.

High intensity heat sources can rapidly heat and melt small, localised volumes of material, and achieve cooling rates that are sufficiently high to suppress crystallisation and hence produce an amorphous structure. For example, laser surface melting can produce cooling rates of $\sim 10^5 \text{ K s}^{-1}$ but electron beam surface melting can achieve even higher cooling rates, typically of the order of $10^8\text{-}10^9 \text{ K s}^{-1}$ [3]. These processes have generated amorphous phases in various Al-, Zr- and Cu-based alloys [4-6]. Large-area electron beam (LAEB) irradiation, a recent variant of electron beam treatment, has several advantages such as a large beam size ($\sim 60 \text{ mm}$ in diameter) which decreases processing time by decreasing the need for overlapping tracks. It has been used to polish mould surfaces [7], increase hardness and wear resistance [8], lower surface roughness, reduce the porosity of sprayed coatings [9] and, as demonstrated in our previous paper [10], generate an amorphous layer when used to melt the surface of a cast Al-Co-Ce alloy. However, cracking of the amorphous layers was found to occur around large, pre-existing particles of the $\text{Al}_8\text{Co}_2\text{Ce}$ phase. Laser processing is a well-known method of microstructural refinement, which

has been applied on many alloys [11, 12]. The aim of the work reported here was to investigate whether a prior laser surface treatment stage could refine the microstructure of as-cast Al-Co-Ce alloy and eliminate the occurrence of this cracking.

2 Materials and methods

2.1 Materials

Bulk crystalline Al-Co-Ce alloy was cast under an argon atmosphere in an induction melting furnace. The composition of the as-cast material was $\text{Al}_{86.0}\text{Co}_{7.6}\text{Ce}_{6.4}$ (at.%) as determined by inductively coupled plasma optical emission spectrometry (ICP-OES) carried out by the Sheffield Assay Office (Sheffield, UK). The alloy composition is in the glass forming range for this type of alloy [13]. 15 mm × 15 mm × 4 mm samples of the as-cast material were cut for laser treatment, the surface was polished using 1 μm diamond paste. Following laser pre-treatment, a raised zone was produced in the centre of each laser track due to surface tension effects. Laser treated samples were then lightly polished again so that flat samples were exposed to the LAEB. After polishing, laser treated material was finally cut into ~5 mm × 5 mm × 4 mm pieces for the LAEB treatment with different number of pulses.

2.2 Laser surface treatment

A YLR-2000SM ytterbium fibre laser (IPG laser, GmbH, Germany) with a wavelength of 1070 nm and a Gaussian (TEM₀₀) beam profile was operated in the continuous wave mode at a power of 2 kW throughout this work. A 600 μm diameter delivery fibre was used with a 192 mm focal length lens, producing a focused spot size with a measured diameter of 952 μm. In order to produce a useful larger beam diameter, the sample was positioned 5 mm below the focus, producing an incident spot size of 3.1 mm in diameter. Overlap of 20% of the track width was

used between successive passes. The samples were clamped onto a moveable stage and treated in an argon atmosphere. Parameters for laser treatment are listed in Table 1.

Table 1 Parameters for laser microstructural refinement.

Distance from focus (mm)	5
Spot size in diameter (mm)	1.5
Sample traverse speed (mm·min ⁻¹)	6000
Overlap (% of track width)	20

2.3 Large area electron beam treatment

A PIKA electron beam surface finishing machine (PF32A) developed by Sodick, Japan was used for LAEB treatment. The detailed information of this machine was described in Walker's work [14]. The electron beam has a diameter of approximately 60 mm. The pulse interval and pulse duration of the electron beam are 11 s and 2-3 μ s, respectively. Throughout this work cathode voltage, anode voltage and solenoid voltage were kept constant at 35 kV, 5 kV and 1.5 kV, respectively. Under the above working conditions, the electron beam has been reported to have an energy density of approximately 6-10 J/cm², varying with distance from the centre of the electron beam [15]. Due to the small specimen size used in this study, the energy density on the whole sample surfaces can be considered constant. The distance between the sample surface and the electron beam source was approximately 300 mm. Before irradiation, the samples were fixed in a clamp on the sample stage, with two sides in contact with the clamp and a ~10 mm gap above the sample stage. Both as-cast and laser pre-treated samples were exposed to 8, 25 and 150 pulses of electron beam irradiation.

2.4 Microstructural characterisation

Before and after laser treatment, X-ray diffraction (XRD) was conducted using a Siemens D500 X-ray diffractometer ($\text{CuK}\alpha$) with a step size of 0.02° and a time per step of 2 s. After electron beam surface treatment, glancing angle XRD (GAXRD) was undertaken using a Bruker D8 Advance diffractometer ($\text{CuK}\alpha$) was carried out to analyse the treated surface layer in isolation from the bulk alloy. GAXRD patterns were collected with a step size of 0.02° , a dwell time of 8 s per step and a 2° angle of incidence. AbsorbDX 1.1 software was used to calculate GAXRD penetration depth. These calculations showed the, 90% contribution, X-ray penetration depth varied with 2θ , ranging from $1.142\ \mu\text{m}$ to $1.260\ \mu\text{m}$ as 2θ varied from 15° to 50° .

Sample surfaces and cross-sections were observed using a FEI XL30 scanning electron microscope (SEM) using backscattered electrons (BSE) to form the image. The semi quantitative composition of different phases was determined by energy dispersive X-ray spectroscopy (EDS). Image analysis was performed using “Image J” software to characterise the laser track, including width and thickness of the track as well as size and spacing of the refined phase. The length of surface cracks were also measured using “Image J” based on four SEM images with magnifications of $300\times$, each image covering an area of $970\ \mu\text{m}$ by $730\ \mu\text{m}$. Measured cracks had a minimum width of $\sim 1.5\ \mu\text{m}$. The crack density was calculated through dividing the total measured length of all surface cracks by the total image area analysed, thereby determining the crack length per unit area. After measurements, the average value and standard derivation of crack density were calculated. For track width and depth and size and spacing of the refined phase, five measurements were conducted for each sample, again the results presented are the average and standard deviation.

3 Results

3.1 Microstructural characterisation of as-cast alloy

The as-cast Al-Co-Ce alloy is a multi-phase crystalline material containing four distinct phases and a two phase eutectic (Figure 1a and Table 2) based on the microstructure observation and EDS analysis. XRD showed the presence of Al, $\text{Al}_{11}\text{Ce}_3$ and $\text{Al}_8\text{Co}_2\text{Ce}$ (Figure 2). From a combination of the EDS and XRD results, the bright white phase 1 is identified as $\text{Al}_{11}\text{Ce}_3$, the darkest region 2 is the eutectic consisting of two phases attributed as Al and $\text{Al}_{11}\text{Ce}_3$. EDS results are consistent with the large particles of phase 3 being $\text{Al}_8\text{Co}_2\text{Ce}$. Phase 5 is attributed to be Al_9Co_2 , although this phase is not evident from the XRD analysis. Phase 4 has a clearly distinct contrast level, and hence different average atomic number, compared to both $\text{Al}_8\text{Co}_2\text{Ce}$ and phase 5. It is proposed that phase 4 is Al-rich $\text{Al}_8\text{Co}_2\text{Ce}$ based on the similar atomic ratio of Co:Ce as $\text{Al}_8\text{Co}_2\text{Ce}$.

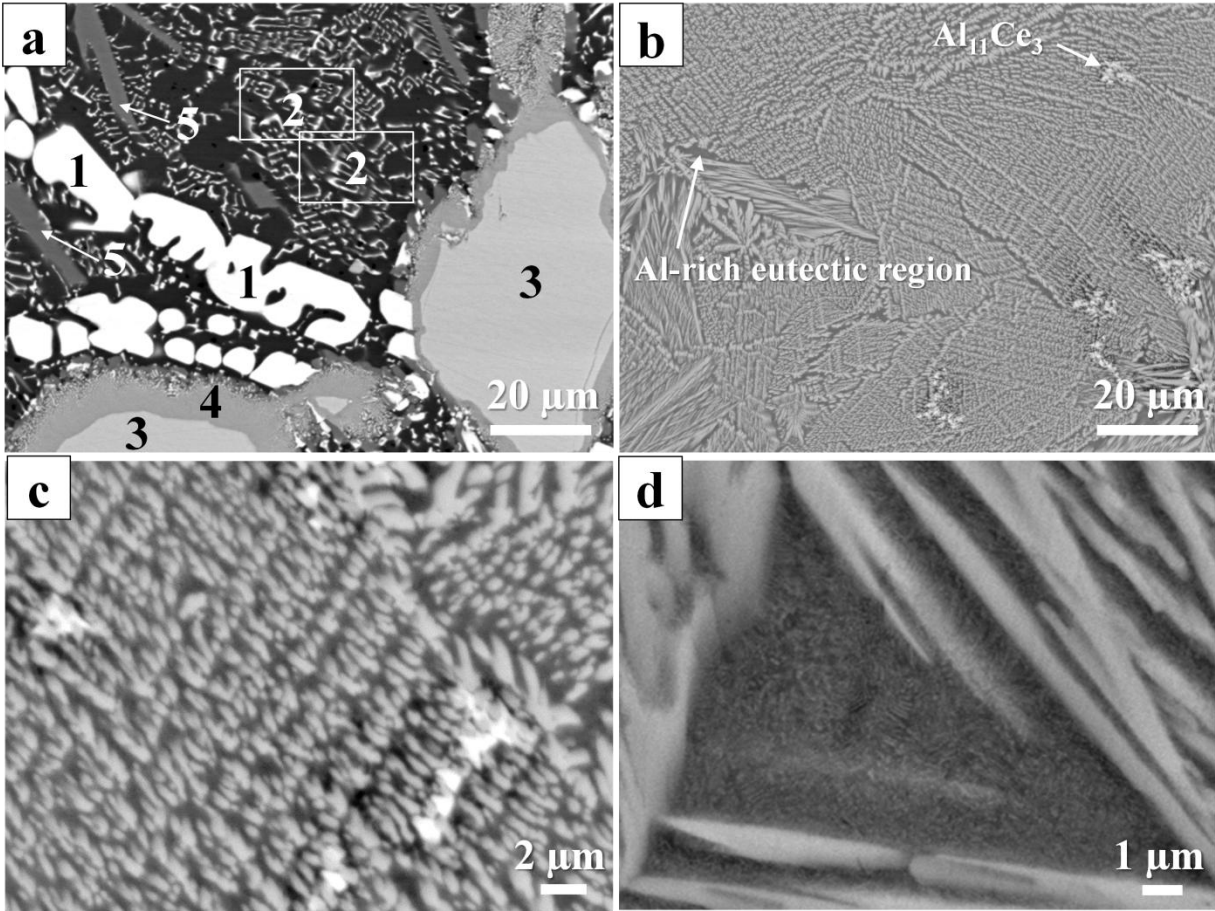


Figure 1 SEM images of as-cast (a) and laser pre-treated sample (b). (c) and (d) are magnified local regions of the laser treated sample showing $\text{Al}_{11}\text{Ce}_3$ particles and Al-rich eutectic regions, respectively.

Table 2 EDS results of different phases in the as-cast material as shown in Figure 1.

Region	Composition (at %)			Probable phase
	Al	Co	Ce	
1	77.1	-	22.9	Primary $\text{Al}_{11}\text{Ce}_3$
2	97.4	-	2.6	Al/ $\text{Al}_{11}\text{Ce}_3$ eutectic
3	72.2	18.2	9.6	$\text{Al}_8\text{Co}_2\text{Ce}$
4	80.6	12.3	7.0	Al -rich $\text{Al}_8\text{Co}_2\text{Ce}$
5	82.9	17.1	-	Al_9Co_2

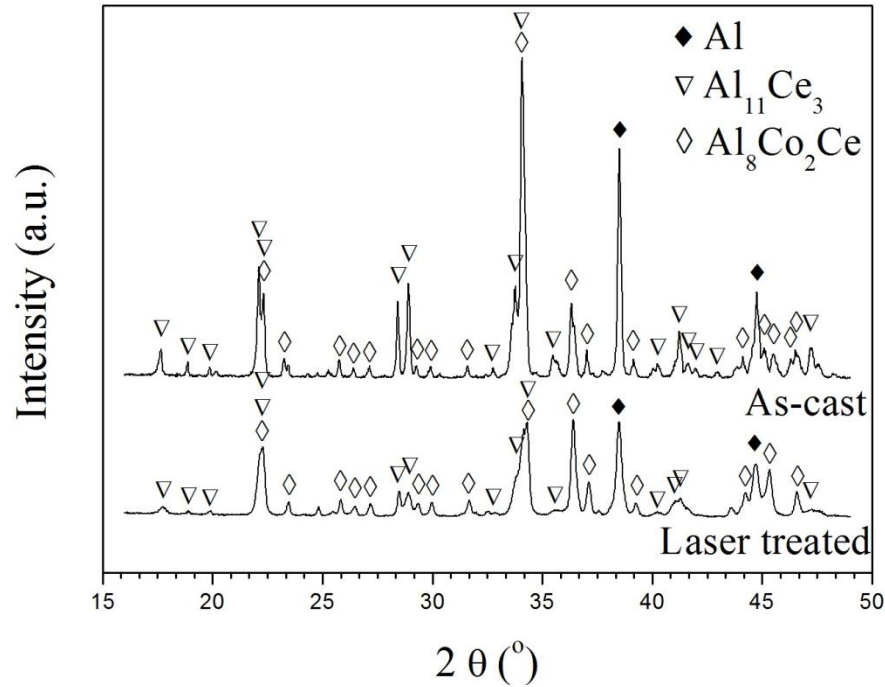


Figure 2 XRD patterns of as-cast and laser pre-treated sample before large area electron beam treatment.

3.2 Microstructural characterisation following laser treatment of as-cast materials

Figure 3 shows the cross section of laser pre-treated sample. It can be seen that laser treatment produced a non-flat surface with ripples. These ripples above the dashed line as shown in Figure 3 were polished flat prior to LAEB treatment. After polishing, the sample still has at least 100 μm refined microstructure, which is far thicker than the possible LAEB treated layer thickness (always less than 10 μm). Generally, laser tracks have a width of 1.4 mm, and a maximum thickness of 333 μm . Compared with the untreated region, laser pre-treated region exhibits an obviously refined microstructure with the disappearance of large $\text{Al}_8\text{Co}_2\text{Ce}$ phase particles. The details of the laser tracks are listed in Table 3.

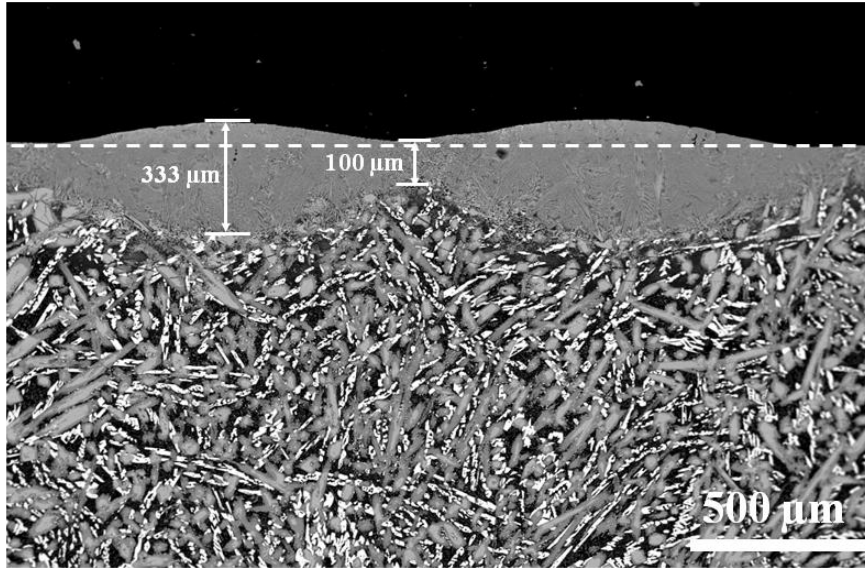


Figure 3 Cross sectional SEM images of laser pre-treated sample. The ripples above the dashed line were polished flat before LAEB treatment.

Table 3 Characterisation of laser pre-treated sample, in each case the standard deviation of results is indicated.

Width of single track (mm)	1.4±0.1
Minimum thickness of laser track (μm)	100±15
Maximum thickness of laser track (μm)	333±27
Particle size of Al ₈ Co ₂ Ce phase in area (length and width, μm)	~ 20±5 × 0.5±0.2
Particle spacing of neighbouring Al ₈ Co ₂ Ce phase (μm)	~0.2±0.1
Composition of Al/Al ₁₁ Ce ₃ eutectic regions (at.%)	Al: 94.4 Co: 0.5 Ce: 5.1

Comparison of Figure 1a and b clearly shows that the microstructure of as-cast Al-Co-Ce alloy was greatly refined, which is also seen in Figure 7. The initial as-cast material has large Al₈Co₂Ce particles, approximately 100 μm × 20 μm in size. While, laser treatment produces a highly refined structure with characteristic feature sizes of approximately 20 μm × 0.5 μm. Accompanied with the decrease in particle size of Al₈Co₂Ce, the spacing between two neighbouring particles also decreases. For the as-cast material, the particle spacing is

approximately 30 μm , while laser pre-treatment reduced this value to approximately 0.2 μm . In addition, for the sample subjected to laser pre-treatment, very few particles of primary $\text{Al}_{11}\text{Ce}_3$ phase were observed in the treated samples (Figure 1b and Figure 1c). Eutectic regions are also found in laser pre-treated sample (Figure 1b and Figure 1d). Bright sub-micron lamellar phases were seen distributed in the darker matrix, which is similar to that seen in the as-cast material, i.e. bright $\text{Al}_{11}\text{Ce}_3$ phase distributed in a largely pure Al phase. The overall composition of this eutectic region in the laser treated sample was analysed by EDS. Result shows a higher content of Ce compared to that in the as-cast material (Table 2 and Table 3). It should also be noted that laser pre-treatment completely eliminated the Al_9Co_2 phase present in the as-cast material.

Figure 2 also shows the XRD pattern of laser treated sample. It can be seen that the laser treated sample still consists of three main phases, including Al, $\text{Al}_{11}\text{Ce}_3$ and $\text{Al}_8\text{Co}_2\text{Ce}$. However, compared with the as-cast material, the amount of the $\text{Al}_{11}\text{Ce}_3$ phase was reduced by the laser pre-treatment with the decreased ratio of the intensity of the strongest $\text{Al}_{11}\text{Ce}_3$ peak ($2\theta=34^\circ$) to that of the $\text{Al}_8\text{Co}_2\text{Ce}$ phase ($2\theta=36.5^\circ$). The $\text{Al}_{11}\text{Ce}_3$ peaks in XRD result and Ce element in EDS result of laser pre-treated sample also confirm those eutectic regions are composed of Al and $\text{Al}_{11}\text{Ce}_3$ phase.

3.3 Microstructural characterisation following LAEB of as-cast and laser pre-treated materials

3.3.1 Glancing angle XRD results

Figure 4 shows the glancing angle XRD results of LAEB treated layer with different initial microstructures. Obvious crystalline peaks are seen in the GAXRD spectra of all samples that were LAEB treated without any prior laser treatment (Figure 4a). After 25 pulses the crystalline

peaks have decreased in intensity and an amorphous hump is present at $2\theta \approx 37^\circ$. After 150 pulses the crystalline peaks have reappeared and the amorphous hump is no longer discernable. There are markedly fewer crystalline peaks in the GAXRD spectra of treated samples with laser pre-treatment (Figure 4b). Those peaks that are present are significantly smaller than those in Figure 4 and an amorphous hump is seen at $2\theta \approx 37^\circ$. Several small crystalline peaks can be seen in the GAXRD spectrum of sample which underwent laser pre-treatment and 150 LAEB pulses.

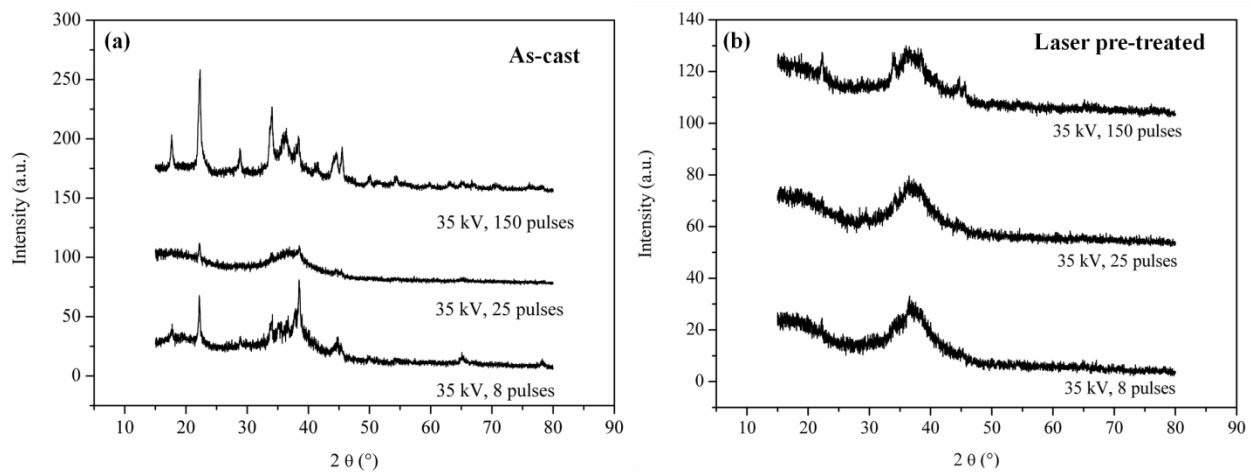


Figure 4 GAXRD spectra of LAEB treated layers with different initial microstructures: (a) as cast and (b) laser treated.

3.3.2 Surface morphology

Figure 5 shows the surface morphology of LAEB treated samples with different initial microstructures. For the samples without any laser pre-treatment, the LAEB remelted surface layer is still markedly heterogeneous after 8 pulses. With increasing numbers of pulses, this layer gradually becomes homogeneous. For the laser pre-treated samples, the remelted layer generally also becomes more uniform in composition with increasing number of pulses. However, it can be seen that this homogenisation is more rapid in the laser pre-treated sample. The composition of LAEB treated sample has become very uniform even after 8 pulses of irradiation. The length

scale over which heterogeneities exist is decreased for the refined microstructures compared to the as-cast material after the same number pulses of LAEB irradiation.

As seen in Figure 5, small, round white particles were observed on the surface of all samples after LAEB treatment. Fewer, larger particles were seen on LAEB treated as-cast material, whereas a higher number of smaller particles were seen for laser pre-treated material. Full investigation of the native of these particles does not form part of the current work but will be considered in our future work.

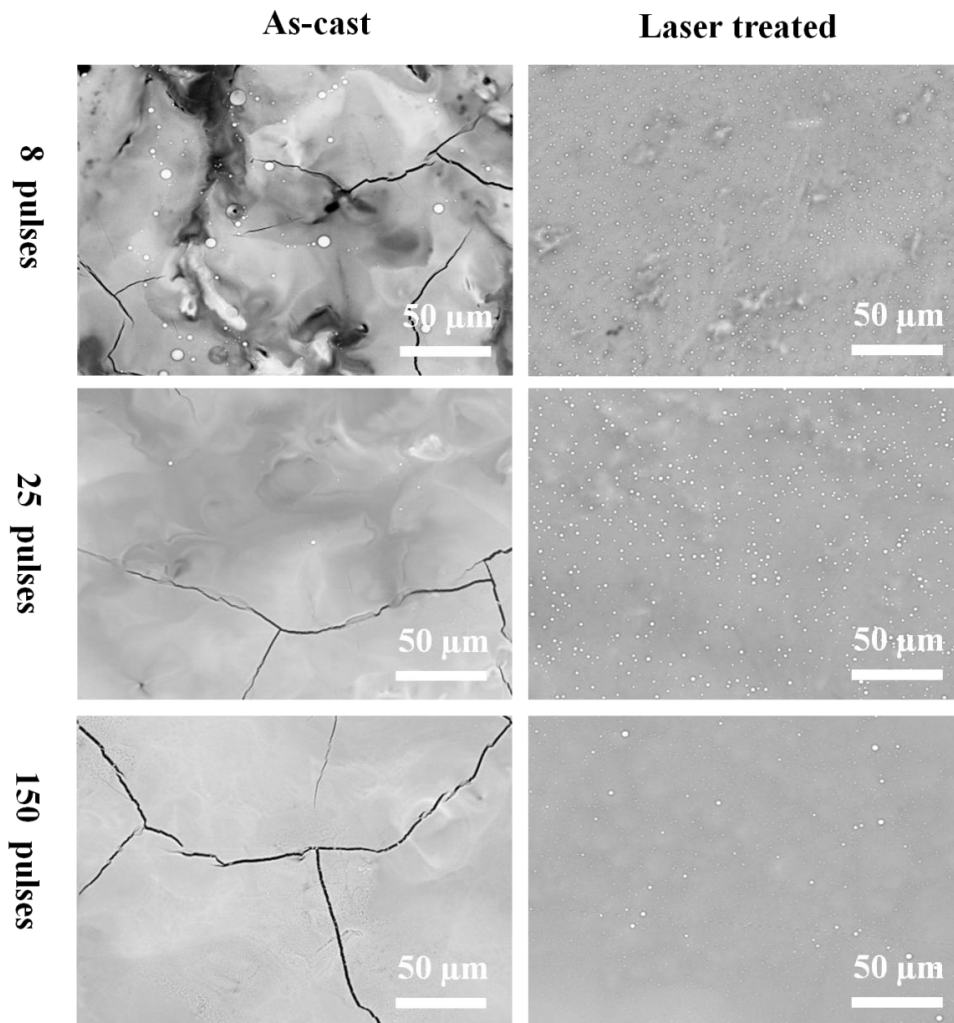


Figure 5 BSE images showing plan views of electron beam treated samples with different initial microstructures and number of LAEB pulses.

For the laser pre-treated sample, the extent of LAEB induced cracking was notably less compared to the as-cast material (Figure 5 and Figure 6). For both type of samples, the extent of cracking increased with the number of pulses. However, for the laser pre-treated sample, the majority of cracking was generated within the first 25 pulses, accompanied by a small increase in the crack density with increasing the number of pulses from 25 to 150. However, in the case of the as-cast material, the majority of cracking formed within the first 8 pulses.

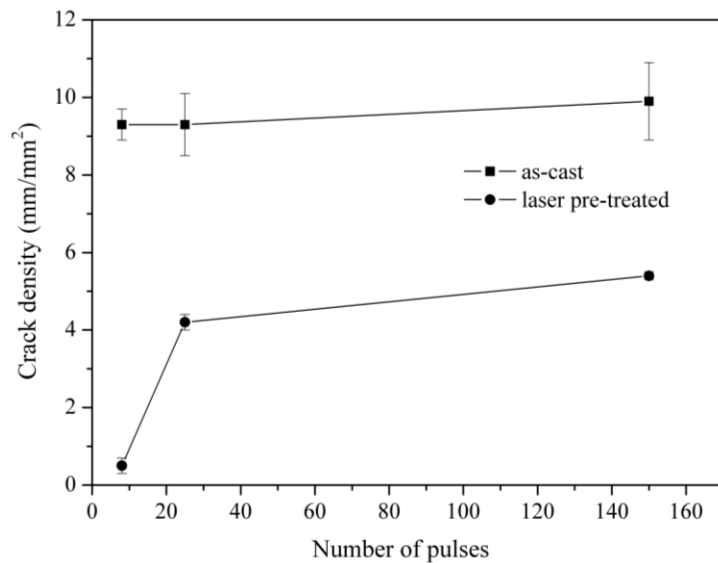


Figure 6 Crack density of treated layers as a function of the number of LAEB pulses.

3.3.3 Cross sectional morphology

Figure 7 shows the cross sections of LAEB treated samples with as-cast and laser pre-treated initial microstructure. For both sample types, there is some variation in the thickness of the treated layer, this is most apparent for the as-cast samples where the thickness of the treated layer varies with the underlying crystalline phase type (Figure 7). In the as-cast samples the treated layer was thinner in regions above $Al_{11}Ce_3$ and Al_8Co_2Ce phases compared to regions above the eutectic, particularly for the 8 pulse sample. The fluctuation of the thickness of the treated layer has a similar lengthscale to the microstructure. There is less variation in the laser refined

structure, resulting in a more regular, straighter interface between the treated layer and bulk material. The homogeneity of the treated layer is increased both by laser microstructural refinement and increasing the number of LAEB pulses. Small crystallites were found in localised regions of the as-cast sample treated with 150 pulses (Figure 8), this is consistent with the XRD results in Figure 4. Such crystallites were not visible in the laser pre-treated sample after the same number of LAEB pulses.

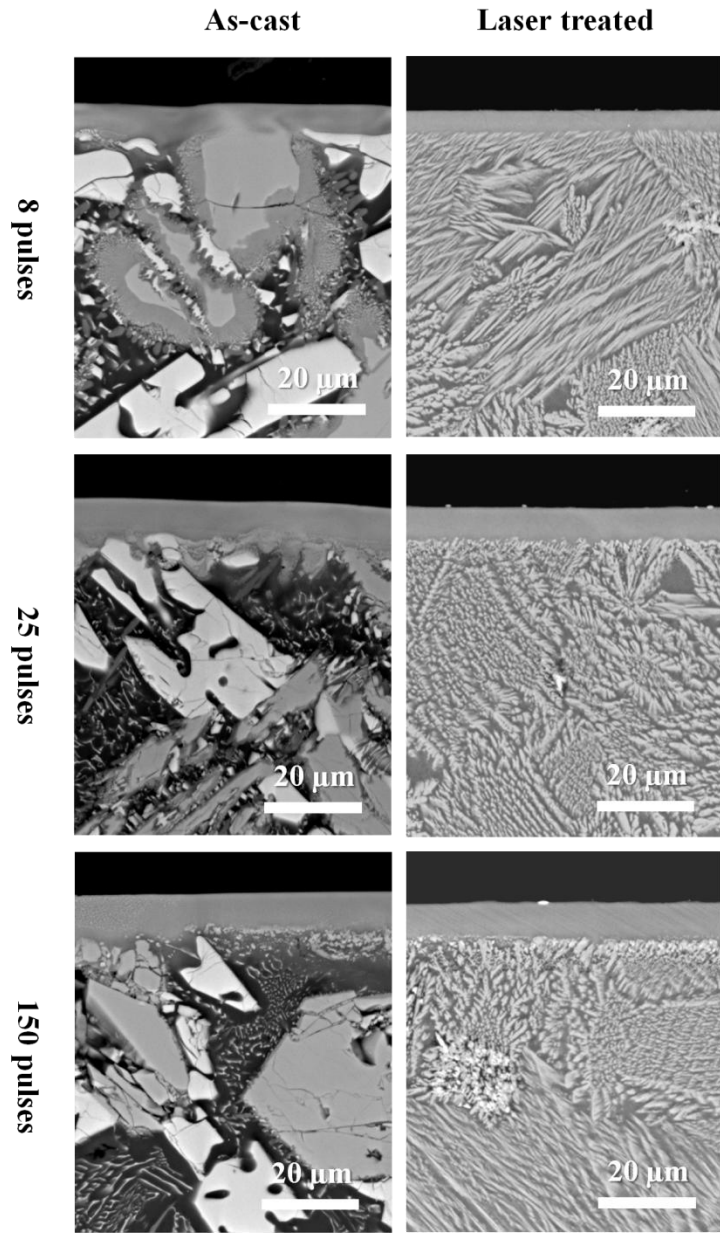


Figure 7 Cross sectional morphology (back scattered electron SEM images) of electron beam treated samples with different initial microstructures and number of LAEB pulses.

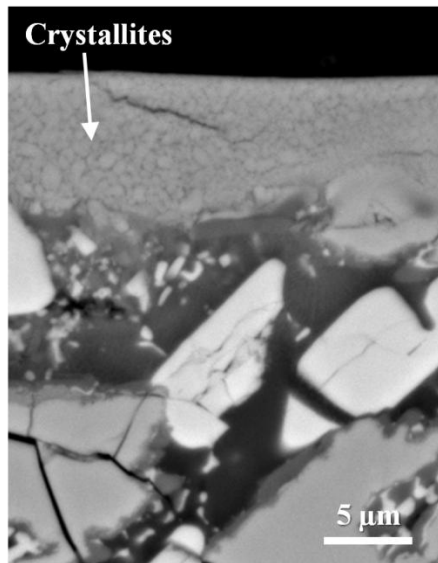


Figure 8 Cross section of LAEB treated as-cast material (35 kV, 150 pulses).

Figure 9 shows the localised cross sectional morphologies of LAEB treated samples (35 kV, 150 pulses) with different initial microstructures. Cracks can be seen in both samples. When the LAEB irradiation was applied to the as-cast material, the crack propagated in the large $\text{Al}_8\text{Co}_2\text{Ce}$ phases over the distance of up to $\sim 70 \mu\text{m}$. However, in the case of laser pre-treated sample, the cracking stopped in the depth of $\sim 20 \mu\text{m}$, which is much shorter than that in the LAEB treated as-cast sample. In addition, the crack in the laser pre-treated sample after LAEB treatment was narrower compared with that in the as-cast material.

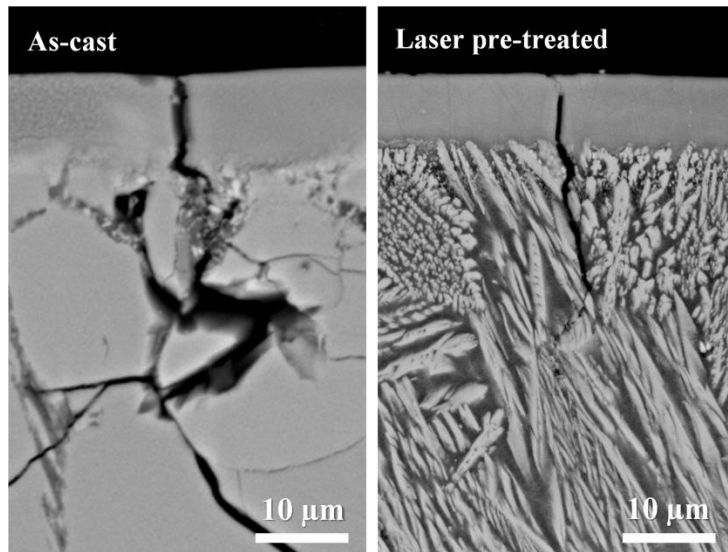


Figure 9 Localised cross sectional morphologies showing the cracks in the LAEB treated samples with different initial microstructures (35 kV, 150 pulses).

4 Discussion

4.1 Microstructural refinement of Al-Co-Ce alloy by the laser pre-treatment

Laser surface melting melts a thin layer of material; this then rapidly cools and solidifies as heat is conducted away by the rest of the material, generating a refined microstructure. The microstructural refinement of the as-cast material was mainly shown by the decrease of particle size and particle spacing of the $\text{Al}_8\text{Co}_2\text{Ce}$ phase. The proportions of the phases present have also been altered by laser treatment due to the high solidification speeds inducing non-equilibrium microstructures, in this case decreasing the amount of primary $\text{Al}_{11}\text{Ce}_3$. The rapid solidification also changed the composition of the Al-rich eutectic region by increasing the content of Ce in the Al-rich region, and eliminated the Al_9Co_2 phase.

4.2 Effect of laser microstructural refinement on the amorphisation of Al-Co-Ce alloy layer

Generally, there are two necessary conditions for the amorphisation of Al-Co-Ce alloy in LAEB treatment. First, the crystalline phases melt and diffuse to obtain a homogeneous composition i.e.

the glass forming composition. This needs a sufficiently high temperature and enough time for the melting and diffusion. Therefore, when low cathode voltage or small number of pulses was used, the alloy cannot be transformed to amorphous state [10]. Second, upon obtaining a homogeneous composition, a fast enough cooling rate is a crucial condition for the alloy to form amorphous phase. The cooling rate following laser surface melting was sufficiently high to refine the microstructure of Al-Co-Ce alloy, but not to generate the amorphous layer. However, LAEB can produce cooling rates that are orders of magnitude larger, typically 10^8 - 10^9 K s⁻¹ [3], these are high enough to enable the amorphous state to be achieved.

For the as-cast material, 8 pulses irradiation provides insufficient time for the molten layer to achieve a uniform composition. However, 25 pulses produces more extensive homogenisation. Therefore, the alloy was amorphised after 25 pulses of irradiation, but not after 8 pulses. In the case of laser treated sample, the alloy microstructure was greatly refined. The time, and hence number of pulses, required for homogenisation, and hence amorphisation of the surface layer, decreases by the decreased particle size, particle spacing of the Al₈Co₂Ce phase. The decreased time required for microstructural homogenisation and amorphisation also reduced the danger of significant bulk sample pre-heating which could affect cooling rate and potentially make amorphisation less likely. Therefore, more extensive homogenisation, and amorphisation, is seen for fewer pulses in the laser refined material. In this present work, the alloy was greatly homogenised and amorphised after only 8 pulses (Figure 5).

The reappearance of crystalline peaks in 150 pulses irradiated as-cast and laser treated material was seen in the glancing angle XRD results. The crystallisation may result from reduced cooling rates due to progressive temperature increase of the substrate with additional pulses [10].

However, crystalline phases are only observed in the SEM image of 150 pulses irradiated as-cast

material (Figure 8) but not in that of laser treated material after the same electron beam irradiation. However, it should be noted that the absence of visible crystalline phases in the SEM image of the latter material may simply be due to a very small, sub-micron, crystal size.

4.3 Effect of laser microstructural refinement on the cracking control of Al-Co-Ce amorphous layer

Figure 10a shows a schematic diagram of the cracking in the LAEB treated as-cast material. The LAEB surface treatment generates a thermal gradient in the material. After solidification, the hot treated layer contracts more than the cold underlying substrate. A tensile stress is generated in the surface, and near surface material, due to this differential contraction. If this tensile stress exceeds the fracture strength of any material in the near surface area then that material will crack.

LAEB treatment of as-cast Al-Co-Ce alloy showed that cracking was correlated with the existence of large $\text{Al}_8\text{Co}_2\text{Ce}$ phase particles. This is due to the brittleness characteristic of this phase [10]. These large and brittle $\text{Al}_8\text{Co}_2\text{Ce}$ phase particles act as easy crack initiation sites in the as-cast material, these particles also provide easy growth paths for the crack propagation, as shown in Figure 9a.

Figure 10b shows the cracking in the laser pre-treated sample after LAEB irradiation. Laser pre-treatment has eliminated the easy crack initiation sites and crack growth paths i.e. microstructural refinement has prevented the formation of large $\text{Al}_8\text{Co}_2\text{Ce}$ phase particles. Hence cracking becomes less likely and the few cracks that do form are shorter and terminate rapidly in the relatively ductile refined microstructure (Figure 9).

It should also be noted that the as-cast material contains a number of different phases which will have different coefficients of thermal expansion. Stresses arising from differential thermal expansion will contribute to crack generation.

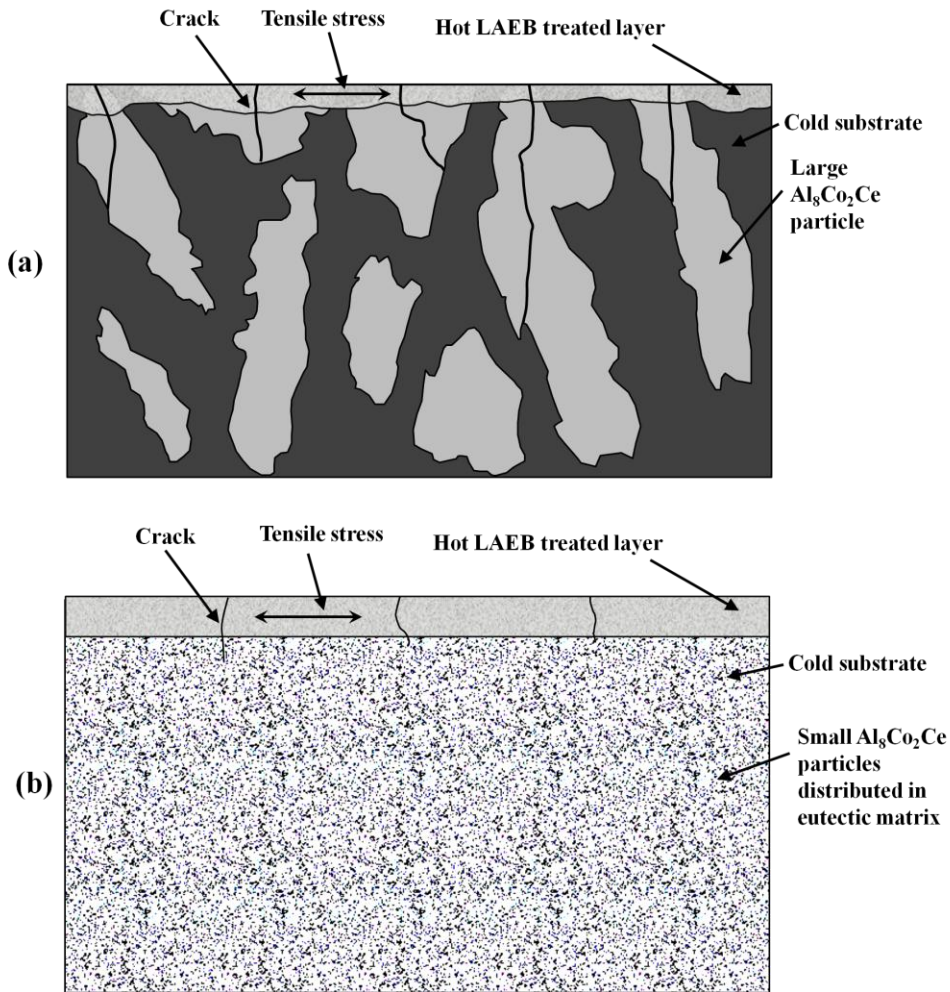


Figure 10 Schematic diagram of cracking in different LAEB treated samples: (a) as-cast sample and (b) laser microstructural refined sample.

4.4 Future work

This work has shown the beneficial effect of laser microstructural refinement. However, it is clear that there are several aspects that require further investigation as well as potential improvements to the process. For example, it would be worth investigating if both

microstructural refinement and amorphisation could be carried out by LAEB treatment. Investigation of residual stresses in the treated layer is also of interest, this would be of particular relevance for the generation of thicker treated layers.

5 Conclusions

- The microstructure of the as-cast $\text{Al}_{86.0}\text{Co}_{7.6}\text{Ce}_{6.4}$ (at.%) alloy was successfully refined by laser pre-treatment. The particle size and spacing of the $\text{Al}_8\text{Co}_2\text{Ce}$ phase are decreased.
- The refined microstructure decreased the number of LAEB pulses required for the homogenisation and amorphisation of Al-Co-Ce alloy.
- Prior laser microstructural refinement successfully decreased the extent of cracking of the amorphous surface layer following LAEB.
- The suppressed cracking of laser pre-treated LAEB treated Al-Co-Ce amorphous layer was due to the removal of large, brittle, $\text{Al}_8\text{Co}_2\text{Ce}$ phase particles.

References

- [1] A.M. Lucente, J.R. Scully, Localized corrosion of Al-based amorphous-nanocrystalline alloys with solute-lean nanocrystals: Pit stabilization, *Journal of the Electrochemical Society*, 155 (2008) C234-C243.
- [2] N. Tailleart, B. Gauthier, S. Eidelman, J.R. Scully, Metallurgical and Physical Factors Controlling the Multi-Functional Corrosion Properties of Pulsed Thermal-Sprayed Al-Co-Ce Coatings, *Corrosion*, 68 (2012) 035006.
- [3] Y. Qin, J. Zou, C. Dong, X. Wang, A. Wu, Y. Liu, S. Hao, Q. Guan, Temperature–stress fields and related phenomena induced by a high current pulsed electron beam, *Nucl Instrum Meth B*, 225 (2004) 544-554.
- [4] J.G. Hoekstra, S.B. Qadri, J.R. Scully, J.M. Fitz-Gerald, Laser surface modification of a crystalline Al-Co-Ce alloy for enhanced corrosion resistance, *Adv Eng Mater*, 7 (2005) 805-809.
- [5] J. Do, C. Jeon, D.-H. Nam, C. Kim, Y. Song, S. Lee, Correlation of Microstructure and Ballistic Performance of Multilayered Zr-based Amorphous Surface Composites Fabricated by High-Energy Electron-Beam Irradiation, *Metall Mater Trans A*, 42 (2011) 1191-1204.
- [6] K. Lee, E. Yun, S. Lee, N.J. Kim, Fabrication of Zr-and Cu-base bulk metallic glass/Cu surface composites by high-energy electron-beam irradiation, *Mater Sci Eng A-Struct*, 408 (2005) 92-101.
- [7] A. Okada, Y. Uno, H. Watanabe, K. Fujiwara, Surface modification of stainless steel for surgical tool by EB-Polishing, *Key Eng Mater*, 407 (2009) 339-342.
- [8] T. Grosdidier, J. Zou, B. Bolle, S. Hao, C. Dong, Grain refinement, hardening and metastable phase formation by high current pulsed electron beam (HCPEB) treatment under heating and melting modes, *J Alloy Compd*, 504 (2010) S508-S511.
- [9] A. Weisenburger, G. Rizzi, A. Scrivani, G. Mueller, J. Nicholls, Pulsed electron beam treatment of MCrAlY bondcoats for EB-PVD TBC systems part 1 of 2: Coating production, *Surf Coat Technol*, 202 (2007) 704-708.

- [10] C.L. Li, J.W. Murray, K.T. Voisey, A.T. Clare, D.G. McCartney, Amorphous layer formation in Al₈₆Co_{7.6}Ce_{6.4} glass-forming alloy by large-area electron beam irradiation, *Appl Surf Sci*, 280 (2013) 431-438.
- [11] C. Kwakernaak, W.G. Sloof, T.J. Nijdam, Microstructure refinement of NiCoCrAlY alloys by laser surface melting, *Metall Mater Trans A*, 37 (2006) 695-703.
- [12] F.A. España, V.K. Balla, A. Bandyopadhyay, Laser processing of bulk Al–12Si alloy: influence of microstructure on thermal properties, *Philos Mag*, 91 (2011) 574-588.
- [13] M.C. Gao, N. Ünlü, M. Mihalkovic, M. Widom, G. Shiflet, Glass formation, phase equilibria, and thermodynamic assessment of the Al-Ce-Co system assisted by first-principles energy calculations, *Metall Mater Trans A*, 38 (2007) 2540-2551.
- [14] J.C. Walker, J. Murray, S. Naranja, A.T. Clare, Dry Sliding Friction and Wear Behaviour of an Electron Beam Melted Hypereutectic Al–Si Alloy, *Tribol Lett*, (2011) 1-10.
- [15] Y. Uno, A. Okada, K. Uemura, P. Raharjo, T. Furukawa, K. Karato, High-efficiency finishing process for metal mold by large-area electron beam irradiation, *Precis Eng*, 29 (2005) 449-455.

Figure captions

Figure 1 SEM images of as-cast (a) and laser pre-treated sample (b). (c) and (d) are magnified local regions of the laser treated sample showing Al₁₁Ce₃ particles and Al-rich eutectic regions, respectively.

Figure 2 XRD patterns of as-cast and laser pre-treated sample before large area electron beam treatment.

Figure 3 Cross sectional SEM images of laser pre-treated sample. The ripples above the dashed line were polished flat before LAEB treatment.

Figure 4 GAXRD spectra of LAEB treated layers with different initial microstructures.

Figure 5 BSE images showing plan views of electron beam treated samples with different initial microstructures and number of LAEB pulses.

Figure 6 Crack density of treated layers as a function of the number of LAEB pulses.

Figure 7 Cross sectional morphology (back scattered electron SEM images) of electron beam treated samples with different initial microstructures and number of LAEB pulses.

Figure 8 Cross section of LAEB treated as-cast material (35 kV, 150 pulses).

Figure 9 Localised cross sectional morphologies showing the cracks in the LAEB treated samples with different initial microstructures (35 kV, 150 pulses).

Figure 10 Schematic diagram of cracking in different LAEB treated samples: (a) as-cast sample and (b) laser microstructural refined sample.

Table captions

Table 4 Parameters for laser microstructural refinement.

Table 5 EDS results of different phases in the as-cast material as shown in Figure 1.

Table 6 Characterisation of laser pre-treated sample.